Acta Crystallographica Section D
Biological Crystallography
ISSN 0907-4449

Growth of (101) faces of tetragonal lysozyme crystals: determination of the growth mechanism

Meirong Li,[a] Arunan Nadarajah[a]* and Marc L. Pusey[b]

[a]Department of Chemical and Environmental Engineering, University of Toledo, Toledo, Ohio 43606, USA, and [b]Biophysics Branch ES76, NASA/Marshall Space Flight Center, Huntsville, Alabama 35812, USA

Correspondence e-mail: arunan.nadarajah@utoledo.edu

Received 15 September 1998
Accepted 16 February 1999

Measurements of the macroscopic growth rates of the (101) face of tetragonal lysozyme crystals indicate an unusual dependence on the supersaturation [Forsythe *et al.* (1999), *Acta Cryst.* D**55**, 1005–1011] similar to that observed for the (110) face. As performed previously for the (110) face, the surface packing arrangement for the (101) face was constructed in this study based on earlier microscopic observations and theoretical analysis of the internal molecular packing. This allowed the minimum growth unit for this face to be identified as a tetramer corresponding to a single turn of helices centered about the 4_3 axes and the minimum growth step to be identified as of unimolecular height. A macroscopic mathematical model for the growth of the (101) face was developed based on the reversible formation of multimeric growth units in solution and the addition of a unit to the crystal face by dislocation and two-dimensional nucleation mechanisms. The calculations showed that the best fits were obtained for tetramer or octamer growth units in this model. This and other evidence suggests that while growth may proceed by a variety of growth units, the average size of these units is between that of a tetramer and an octamer.

1. Introduction

Comprehensive study of the growth rates of the (101) face of tetragonal lysozyme crystals showed that their unusual dependence on the supersaturation had a strong resemblance to the growth behavior of the (110) face (Nadarajah *et al.*, 1995; Forsythe *et al.*, 1999). With increasing supersaturations, these growth rates increase, reach a peak value and then start decreasing. As the supersaturations are lowered, the growth rates decrease rapidly and approach zero asymptotically. This resemblance in the growth-rate trends of the two faces suggests that their growth mechanisms may also be similar. If so, then the approach employed to successfully determine the growth mechanism of the (110) face could also be applied to the (101) face.

The growth mechanism of the (110) face was determined in two different, but complementary, ways. One approach was to analyze the molecular-packing arrangements in the tetragonal lysozyme crystal structure and relate it to the surface-packing arrangement (Nadarajah & Pusey, 1996; Nadarajah *et al.*, 1997; Strom & Bennema, 1997*a*,*b*). This relationship then allowed the molecular-growth mechanism of the crystal face to be deduced and the results to be confirmed from atomic force microscopy (AFM) and electron-microscopy studies. These analyses revealed that tetragonal lysozyme crystals were constructed by helices centered around the 4_3 axes, consisting of four molecules in a single turn (Konnert *et al.*, 1994; Li,

Perozzo *et al.*, 1999). The growth mechanism was shown to proceed by the addition to the (110) face of a variety of growth units corresponding to these helices (Li, Nadarajah *et al.*, 1999).

The second approach involved relating the growth conditions in the nutrient solution to the crystal-growth rates, and determining all the processes in the solution and the crystal face which contribute to the overall growth process (Li *et al.*, 1995; Nadarajah *et al.*, 1997). The formation of the postulated multimeric growth units is likely to occur by a self-association process in the solution. For modeling purposes, we assumed it to be a series of reversible doubling reactions. The crystal-growth process was assumed to be either a dislocation or a two-dimensional nucleation growth mechanism. A mathematical model of the entire process was developed, and from comparisons of the predicted growth rates with the measured ones, the growth unit which gave the best agreement between the two was obtained. The model was then checked for consistency by comparing predictions of process variables from it, such as enthalpies, with those measured by other means.

The application of this dual approach to the (110) face showed that the growth of these faces proceeds by the formation of lysozyme clusters corresponding to the 4_3 helices in solution, followed by their addition to the crystal face by faceted crystal-growth mechanisms. We will apply this approach to the (101) face in this study. Our earlier analyses of crystal packing had already indicated that for this face the growth unit was at least a 4_3 tetramer (Nadarajah & Pusey, 1996). However, precise surface-packing arrangements and the molecular-growth mechanism of this face were not determined. Additionally, no attempt was made to convincingly model the growth rates and obtain the likely growth unit. Both of these goals will be accomplished here, employing the comprehensive growth-rate data previously collected for the (101) face.

2. Growth mechanism and surface morphology

The crystallographic coordinates of chicken egg-white lysozyme in the tetragonal form were obtained from the Protein Data Bank file 193L (Young *et al.*, 1994). The visualization and analysis of the packing arrangements and the intermolecular bonds were accomplished with the the commercial program *QUANTA* (Molecular Simulations Inc., San Diego, USA). The construction of the crystal model involved suitably assembling molecules with the eight unique orientations which make up the unit cell in the $P4_32_12$ space group (*International Tables for Crystallography*, 1983, *Vol. A*, No. 96).

Fig. 1 shows the tetragonal lysozyme crystal with the (101) and (110) families of faces. Fig. 2(*a*) shows the unit cell viewed along the *c* crystallographic axis, with the reference molecule labeled *M* and the other seven molecules labeled *A*–*G*, employing a simplified representation for each molecule (Nadarajah & Pusey, 1996). The space occupied by each lysozyme molecule in the crystal (the asymmetric unit) is a rectangular block of dimensions 28.0 × 28.0 × 37.9 Å as shown in Fig. 2(*b*). This rectangular block of Fig. 2(*b*) and the simplified representation of Fig. 2(*a*) will be used to represent lysozyme molecules in subsequent constructions. In the earlier study, the nearest-neighbor interactions between the molecules were estimated and employed in a periodic bond-chain analysis of the crystal structure (Nadarajah & Pusey, 1996). The results from that study will be employed here in constructing the detailed surface morphology of the (101) face.

Figs. 3(*a*) and 3(*b*) show the [010] and the [001] projections of the tetragonal structure constructed from the representations of lysozyme molecules employed in Figs. 2(*a*) and 2(*b*). These figures indicate what was established at length by our earlier study: the four-molecular unit *M*–*C*–*A*–*B*, centered around the 4_3 crystallographic axis, can be regarded as a building block for the entire crystal (Nadarajah & Pusey, 1996). The four-molecular *D*–*F*–*E*–*G* unit is the same as the *M*–*C*–*A*–*B* unit, but oriented in the opposite direction along the *c* axis, and the entire molecular-packing arrangement in the crystal can be constructed from the *M*–*C*–*A*–*B* unit. It was also shown that the 4_3 helix is formed by strong bonds and that crystal growth is likely to proceed in a manner which preserves this unit's structure. These predictions were confirmed by AFM scans which showed that the (110) faces are formed by planes corresponding to this construction (Konnert *et al.*, 1994; Li, Perozzo *et al.*, 1999). Further confirmation was provided by a recent study of the crystal-packing arrangement employing a somewhat different approach (Strom & Bennema, 1997*a*,*b*). This study also showed that the building blocks of tetragonal lysozyme crystals were tetramers. Thus, growth of the (101) face by a mechanism involving the formation of incomplete 4_3 helices is unlikely.

For the case of the (101) face, construction of the molecular-packing arrangement with these 4_3 tetramer units results in the formation of surfaces with jagged edges, as shown in Figs. 3(*a*) and 3(*b*). Coincidentally, this construction produces edge-to-edge dimensions of 79.1, 79.1 and 37.9 Å in the *a*, *b* and *c*

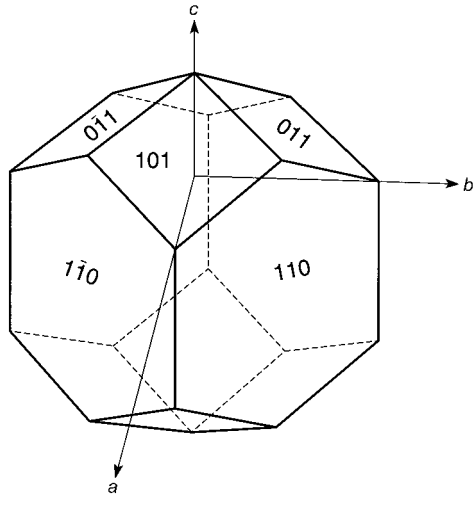

Figure 1
Illustration of the normal growth habit of tetragonal lysozyme crystals showing some of the faces.

crystallographic directions, respectively, which are the unit-cell dimensions in these directions (Steinrauf, 1959). Construction of this face with incomplete 4_3 helices to obtain single molecular edges is possible, as shown in Fig. 3(*c*). This will result in surfaces with less relief and smaller edge-to-edge dimensions than those of the unit cell in at least one direction (Fig. 3*c*). Electron microscopy and AFM studies of the (101) face confirm nicely the construction of the (101) face by the 4_3 helix; they show that this face displays high relief with jagged edges and that the measured edge-to-edge dimensions correspond to the unit-cell dimensions (Durbin & Feher, 1990; Durbin & Carlson, 1992). Low relief or molecular (as opposed to unit-cell) edge-to-edge dimensions were not observed on this face by these studies.

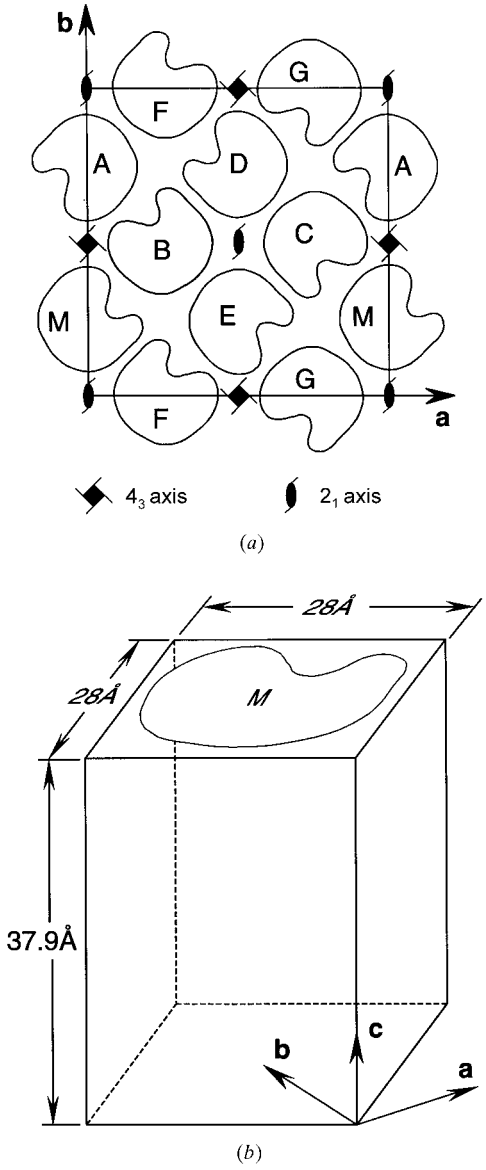

Figure 2
Simplified representation of lysozyme molecules in tetragonal crystals with a space group of $P4_32_12$. (*a*) The unit cell of tetragonal lysozyme showing the eight molecules. The reference molecule is labeled *M* and the other seven are labeled *A*–*G*. The fourfold and twofold screw axes are shown. (*b*) The space occupied by the reference molecule *M*. Such rectangular blocks can be used to represent the molecules themselves in the construction of packing arrangements on the crystal face.

The above considerations, coupled with the observation that growth steps on the (101) face are unimolecular (Durbin & Feher, 1990; Durbin & Carlson, 1992), require that the crystallizing units for this face be the 4_3 tetramers. In order to demonstrate this, we will first show that a monomeric growth mechanism is inconsistent with microscopic observations. This is illustrated in Fig. 4, which shows the (101) face with a growth layer corresponding to monomeric growth. Not only will such a growth layer produce an incomplete 4_3 helix, but it will also cause the growth step height to be $0.5d_{101}$ or 17.1 Å. This should correspond to a half-molecular growth layer, which is not observed experimentally. Growth units of at least tetramer size are needed to preserve the completeness of the 4_3 helices in the crystal, which is a requirement for both the (110) and (101) faces (Nadarajah & Pusey, 1996; Strom & Bennema, 1997*a*,*b*). As mentioned previously, only complete 4_3 helices were found on the (110) face in AFM investigations (Konnert *et al.*, 1994; Li, Perozzo *et al.*, 1999). This requirement also rules out larger crystallizing units for this face, as this would have resulted in the growth steps being multi-layered.

Figs. 3(*a*) and 5 show the (101) face with a growth layer corresponding to a 4_3 tetramer crystallizing unit. The mechanism not only preserves the integrity of the 4_3 helix, but also ensures that the growth step height is d_{101} or 34.2 Å. Thus, it is the most likely structure for the growth layer. The step height presumably corresponds to the unimolecular growth layers observed on this face (Durbin & Feher, 1990; Durbin & Carlson, 1992). Unfortunately, Durbin and coworkers do not report growth step heights as were reported for the (110) face by Konnert *et al.* (1994). Nevertheless, 34.2 Å is much closer than 17.1 Å to the 28.0 × 28.0 × 37.9 Å dimensions of single lysozyme molecules as shown in Fig. 2(*b*). This would suggest that the unimolecular growth steps observed on the (101) face are of 34.2 Å height, but this needs to be confirmed by systematic height measurements.

The growth mechanism of the (101) face differs from that of the (110) face in the size restriction of the growth unit to only a tetramer for single-layer growth. The relative smoothness of the (110) face allows the addition of units of many sizes even for a single growth layer (Nadarajah & Pusey, 1996; Nadarajah *et al.*, 1997). As long as the growth units conform to the bimolecular growth step height on the (110) face, their maximum size is restricted more by their stability in solution, rather than by the structure of the growth step. In contrast, the jagged step-like structure of the (101) face does not readily allow the incorporation of growth units larger than a tetramer, as seen from Figs. 4 and 5. While it restricts the growth-unit size, this high-relief structure facilitates the attachment of all manner of molecules onto these faces. This makes it likely that this face is easily poisoned by misaligned lysozyme molecules and other macromolecular impurities, giving rise to macro-steps consisting of multiple growth layers. Formation of these macrosteps on both (110) and (101) faces can cause growth to proceed by the addition of larger growth units. Thus, for both faces growth will proceed by growth units which are larger

than the minimum tetramer size. However, the greater restrictions on the allowed growth-unit size for the (101) face is likely to cause the average size of the units attaching to it to be smaller than that for the (110) face.

The above arguments are validated by experimental observations. Recent time-resolved AFM studies of millisecond resolution showed that it was possible to observe individual growth events and measure the size of the growth unit for the (110) face (Li, Nadarajah *et al.*, 1999). Many growth units were observed to participate in the process with tetramers the minimum size, all corresponding to 4_3 helices. Some units were as large as dodecamers. Earlier AFM and electron-microscopy studies have shown that growth by multilayers is a common occurrence on both (101) and (110) faces (Durbin & Feher, 1990; Durbin & Carlson, 1992; Konnert *et al.*, 1994). Additionally, several studies have shown that the (101) face grows faster than the (110) face at lower supersaturations and grows more slowly than the (110) face at higher supersaturations (Durbin & Feher, 1986; Forsythe *et al.*, 1999). As we will show below, this trend can be explained if the averaged size of the units participating in the growth process is smaller for the (101) face than for the (110).

3. Modeling the growth rates

The arguments made in the previous section suggest that growth on the (101) face normally proceeds by the addition of tetramer or larger units. Such crystallographic analyses and microscopic scans of the crystal face can indicate the crystallizing unit for growth, but not how this unit is formed. For example, the crystallizing unit could be nucleated on the crystal face during growth. For the case of tetramer units, this would require the correctly oriented deposition of four lysozyme molecules on the growth step on less than millisecond timescales (Li, Nadarajah *et al.*, 1999). Such events are unlikely to be the norm and even less so for larger units. It is far more likely that these units are formed by sequential bimolecular self-association reactions in the bulk solution which then add to the growing crystal face, as illustrated in Fig. 5. Such a mechanism is also suggested by studies showing the presence of clusters in lysozyme solutions under crystallization conditions (Pusey, 1991; Behlke & Knespel, 1996; Minezaki *et al.*, 1996; Wilson *et al.*, 1996).

In our earlier models for the growth of the (110) face, it was assumed that the sequential self-association process could be represented by a series of reversible doubling reactions given by

$$\text{monomer} \rightleftharpoons \text{dimer} \rightleftharpoons \text{tetramer} \rightleftharpoons \text{octamer} \rightleftharpoons \text{higher order } n\text{-mers}. \quad (1)$$

The growth units formed in this manner are transported to the interface, followed by their attachment to the crystal face. Given that the self-association process involves the stronger set of molecular interactions and smaller reactants, it is likely to be the faster step in the overall growth process (Nadarajah & Pusey, 1996; Nadarajah *et al.*, 1997). The attachment of a large growth unit to the crystal face by weaker intermolecular bonds is likely to be the slow rate-limiting step. This is in accordance with the observation that tetragonal lysozyme growth is limited by surface kinetics. However, the growth model for the (110) face also assumed that there was only one growth unit among those given in (1), which was determined from the best fit to the measured growth-rate data (Li *et al.*, 1995). From this analysis, it was concluded that octamers were the predominant growth unit for the (110) face.

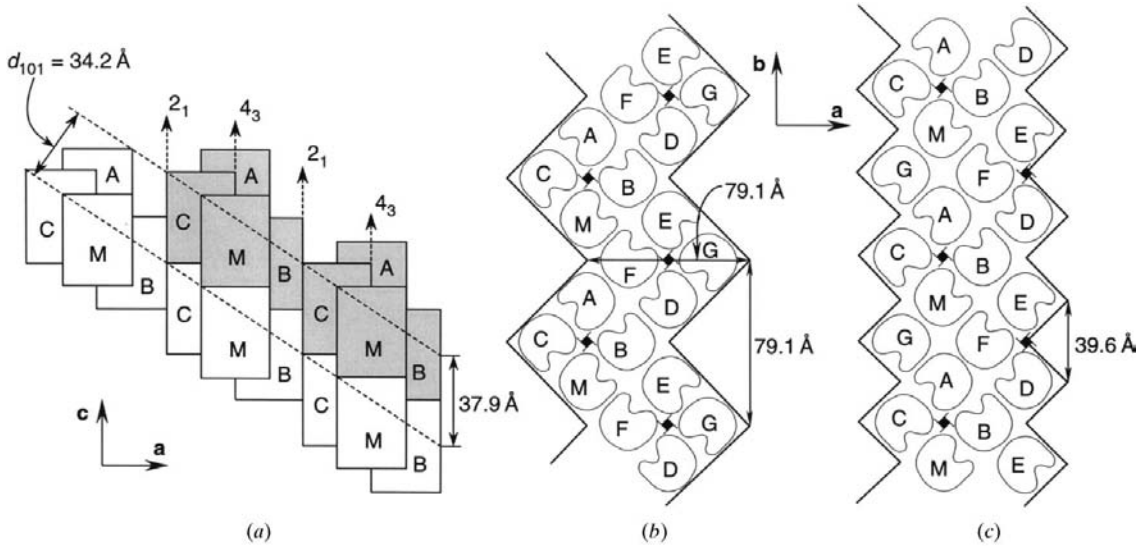

Figure 3
Construction of a growth step on the (101) face. (*a*) The growth step constructed employing complete 4_3 helices, as viewed along the *b* axis. The second layer forming the step is shown in gray and has a height of 34.2 Å. (*b*) The growth step for complete 4_3 helices shown in (*a*), as viewed along the *c* axis. This produces a face with high relief as given by the edge-to-edge dimensions corresponding to the unit-cell dimensions. (*c*) Growth step constructed without completing the 4_3 helices, but for the same step height as in (*a*) and (*b*), as viewed along the *c* axis. The face is smoother with smaller edge-to-edge dimensions.

The recent AFM study showed that this is not the case and that many growth units are involved (Li, Nadarajah *et al.*, 1999). As discussed previously, it is likely that this will also be true for the (101) face. However, macroscopic models do serve a useful purpose even if they cannot identify the individual growth units. The octamer growth unit identified by the model for the (110) face represents the average size of all units participating in the growth process. This means that large growth units are involved in the growth process, which explains the need for high supersaturations to obtain appreciable crystal growth rates. For the (101) face, by identifying the average growth-unit size, such a model can explain the growth-rate differences between it and the (110) face which lead to the formation of flat crystals at high supersaturations and long needles at low supersaturationss.

In this study, the self-association process given in (1) was assumed to be at equilibrium and the distribution of lysozyme clusters was determined as performed in our earlier study for the (110) face (Li *et al.*, 1995). Equilibrium constants were defined for the above series of reactions. For the formation of $2i$-mers from i-mers the equilibrium constant $K_{i\rightarrow 2i}$ is given by

$$K_{i\rightarrow 2i} = K^0_{i\rightarrow 2i}\exp(-\Delta H_{i\rightarrow 2i}/RT) = (C^{1/2}_{2i}/C_i)^{1/i}, \qquad (2)$$

where C_i is the i-mer concentration, T is the temperature, $K^0_{i\rightarrow 2i}$ is the pre-exponential constant and $\Delta H_{i\rightarrow 2i}$ is the heat of reaction, with all variables defined per mole of monomeric lysozyme. The enthalpies and the pre-exponential constants were determined in our earlier study from data fits to the measured (110) growth rates, assuming a dislocation growth model (Li *et al.*, 1995). The results agreed well with the enthalpies estimated from the solubility data (Cacioppo & Pusey, 1991) and estimates of the equilibrium constant for the formation of dimers from aggregation studies (Wilson *et al.*, 1996). These values of the equilibrium constants and enthalpies will be utilized in this study to determine the cluster distributions, as the same distributions can also be assumed to exist in solution for the growth of (101) faces.

The growth rate R of a dislocation hillock is given by

$$R = pv, \qquad (3)$$

where p is the hillock slope and v is the tangential growth-step velocity given by

$$v = \beta\Omega(C - S), \qquad (4)$$

where C is the solute concentration, S is the solubility at that temperature, β is the kinetic coefficient and Ω is the volume occupied by the growth unit in the crystal (Chernov, 1984, 1988). For isolated growth hillocks p is given by

$$p = hkT\sigma/19\Omega\alpha, \qquad (5)$$

where h is the growth step height, T is the temperature, σ is the supersaturation defined as $\ln(C/S)$ and α is the step free energy.

For two-dimensional nucleation the commonly used model of the growth rate is given by Chernov (1984, 1988),

$$R = \text{constant} \times C^{1/3}\sigma^{1/6}(C - S)^{2/3}\exp(\pi h\Omega\alpha^2/3k^2T^2\sigma). \quad (6)$$

As written, (3)–(6) are valid only for monomer growth from monodisperse solutions. For aggregate growth on the (110) face of tetragonal lysozyme they will have to be modified, with C, S and σ being replaced by C_n, S_n and σ_n. Here, C_n is the n-mer growth-unit concentration in the nutrient solution, S_n is the concentration of that n-mer at saturation and σ_n is the n-mer supersaturation defined as $\ln(C_n/S_n)$. Some of the parameters, such as Ω, will also have to be modified for n-mer growth.

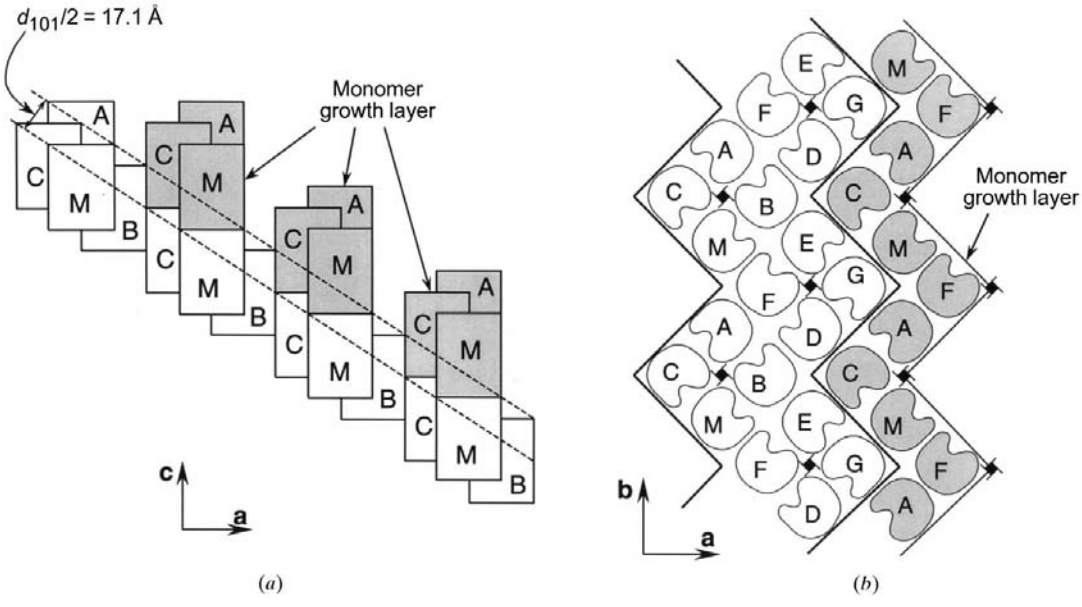

Figure 4
Construction of a growth step formed by a monomer growth layer on the (101) face: (*a*) view along the *b* axis, (*b*) view along the *c* axis. Such a layer can produce the observed edge-to-edge dimensions, but the step height is now only 17.1 Å and incomplete 4_3 helices are formed.

In assessing the above models, comparisons were made with measured averaged growth rates of the (101) face at three sets of conditions: pH 4.6/3% NaCl, pH 4.0/5% NaCl and pH 5.0/5% NaCl (Forsythe *et al.*, 1999). At each lysozyme concentration and temperature, the distribution of clusters was determined as described previously (Li *et al.*, 1995). The values of the equilibrium constants and enthalpies used in the calculation were taken from the earlier study and are listed here in Table 1. Growth of the

(101) face by three different growth units were considered: monomers, tetramers and octamers. The measured growth rates were plotted against the various functional relationships given by the monomer (monodisperse), tetramer and octamer versions of (3)–(6).

As discussed in §2 and earlier studies (Nadarajah & Pusey, 1996; Strom & Bennema, 1997*a*,*b*), the smallest growth unit for both the (110) and (101) faces is a tetramer. This was also demonstrated for the (110) face by the AFM study (Li, Nadarajah *et al.*, 1999). Some calculations were carried out for dimers, but as expected they did not produce any agreement with the measured growth-rate data. Thus, growth units smaller than tetramers are not considered in the following section.

Table 1
Values of parameters in (2) used to determine the molecular clusters in lysozyme solutions at various conditions.

The values were taken from Li *et al.* (1995).

Parameter/ condition	pH 4.6/ 3% NaCl	pH 4.0/ 5% NaCl	pH 5.0/ 5% NaCl
$K^0_{1\rightarrow 2}$ ($M^{-1/2}$)	4.7×10^{-6}	8.7×10^{-6}	4.4×10^{-3}
$K^0_{2\rightarrow 4}$ ($M^{-1/4}$)	1.5×10^{-4}	1.3×10^{-3}	7.0×10^{-3}
$K^0_{4\rightarrow 8}$ ($M^{-1/8}$)	6.7×10^{-3}	1.1×10^{-2}	1.4×10^{-2}
$K^0_{8\rightarrow 16}$ ($M^{-1/16}$)	5.6×10^{-2}	6.0×10^{-2}	5.9×10^{-2}
$\Delta H_{1\rightarrow 2}$ (kJ mol^{-1})	−37.7	−37.7	−20.9
$\Delta H_{2\rightarrow 4}$ (kJ mol^{-1})	−25.1	−20.9	−16.7
$\Delta H_{4\rightarrow 8}$ (kJ mol^{-1})	−14.2	−13.0	−12.6
$\Delta H_{8\rightarrow 16}$ (kJ mol^{-1})	−7.9	−7.9	−9.2

4. Results and discussion

From (3)–(5) for dislocation growth, the growth rates are expected to be a linear function of $T\sigma_n(C_n - S_n)/T_{\rm av}$ for an n-mer growth unit. (Here, $T_{\rm av}$ is 286 K and is employed to make the abscissa in Figs. 6–11 dimensionless with respect to temperature.) The measured growth rates were plotted against $T\sigma(C - S)/T_{\rm av}$, $T\sigma_4(C_4 - S_4)/T_{\rm av}$ and $T\sigma_8(C_8 - S_8)/T_{\rm av}$ for each of the three sets of conditions. These are shown in Figs. 6, 7 and 8, respectively.

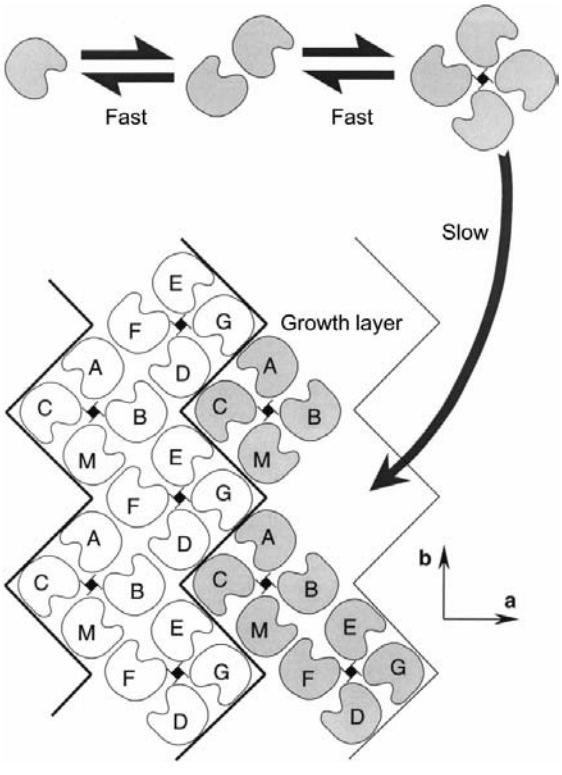

Figure 5
The growth mechanism of the (101) face by a growth layer corresponding to complete 4_3 helices. The growth of this layer occurs by the addition of 4_3 tetramers formed in solution by a sequential self-association process. The formation of the tetramer unit involves the association of smaller units by stronger interactions, making this a fast step. The addition of the tetramer to the growth layer involves weaker interactions and a larger unit, causing this to be the slow rate-determining step.

For the case of pH 4.6/3% NaCl shown in Fig. 6, the assumption of monomer or tetramer growth units clearly does not produce the expected linear behavior of the measured growth rates. Considering monomer growth from monodisperse solutions, when the measured growth rates are plotted against $T\sigma(C - S)/T_{\rm av}$ the resulting curve does not even pass through the origin. This is also the case when tetramer growth from polydisperse solutions is considered by plotting the growth rate against $T\sigma_4(C_4 - S_4)/T_{\rm av}$. In other words, for these two cases the measured growth rates deviate from expected behavior for dislocation growth at lower σ. However, it is at the low σ that dislocation growth is expected to prevail. We can conclude from this that the growth rates do not follow the dislocation growth model for averaged growth units which are of monomer or tetramer size.

Fig. 6 shows that when the averaged growth unit is assumed to be an octamer and the growth rates are plotted against $T\sigma_8(C_8 - S_8)/T_{\rm av}$, the curve passes through the origin. It also shows a linear dependence at lower σ and deviations from linearity at higher σ. Both these are expected trends for dislocation growth. At larger σ these deviations from linearity are expected, as growth proceeds predominantly by two-dimensional nucleation. Fig. 7 shows the same dislocation growth plots for the case of pH 4.0/5% NaCl. Once again it is clear that growth does not proceed by monomer- or tetramer-averaged growth units, while the octamer unit shows agreement at lower σ. The same conclusions can also be drawn from Fig. 8 for the case of pH 5.0/5% NaCl.

From (6), for two-dimensional nucleation growth the growth rates are expected to be linear with $C_n^{1/3}\sigma_n^{1/6}(C_n - S_n)^{2/3}\exp(-qT_{\rm av}^2/T^2\sigma_n)$ for an n-mer averaged growth unit. Here q is $\pi h\Omega\alpha^2/3k^2T_{\rm av}^2$, which is obtained from a least-squares fit of $\ln[R/C_N^{1/3}\sigma_n^{1/6}(C_n - S_n)^{2/3}]$ with $T_{\rm av}^2/T^2\sigma_n$. The growth rates are then plotted for each of the three sets of conditions and are shown in Figs. 9, 10 and 11. The corresponding values of q are given in the figure captions.

Fig. 9 shows that for the case of pH 4.6/3% NaCl, assuming monomer (monodisperse) or octamer growth results in deviations from expected trends for two-dimensional nucleation growth. When the measured growth rates are plotted

against $C^{1/3}\sigma^{1/6}(C-S)^{2/3}\exp(-qT_{av}^2/T^2\sigma)$ or $C_8^{1/3}\sigma_8^{1/6}\times(C_8-S_8)^{2/3}\exp(-qT_{av}^2/T^2\sigma_8)$, the resulting curve is linear at low σ, while at high σ a maximum value is reached followed by decreases in the growth rates. Since two-dimensional nucleation growth is expected to occur mostly at high σ, these deviations from expected trends at high σ clearly suggest that the averaged growth units here are neither monomers nor octamers. When tetramer growth units are considered, by plotting the growth rates against $C_4^{1/3}\sigma_4^{1/6}(C_4-S_4)^{2/3}\times\exp(-qT_{av}^2/T^2\sigma_4)$, the expected linear behavior is obtained. This suggests that for pH 4.6/3% NaCl the growth proceeds by two-dimensional nucleation at high supersaturations with tetramers as the averaged growth units.

The average growth-unit size is different for the other two conditions, however. Figs. 10 and 11 show that when the growth rates are plotted against $C_4^{1/3}\sigma_4^{1/6}(C_4-S_4)^{2/3}\times$

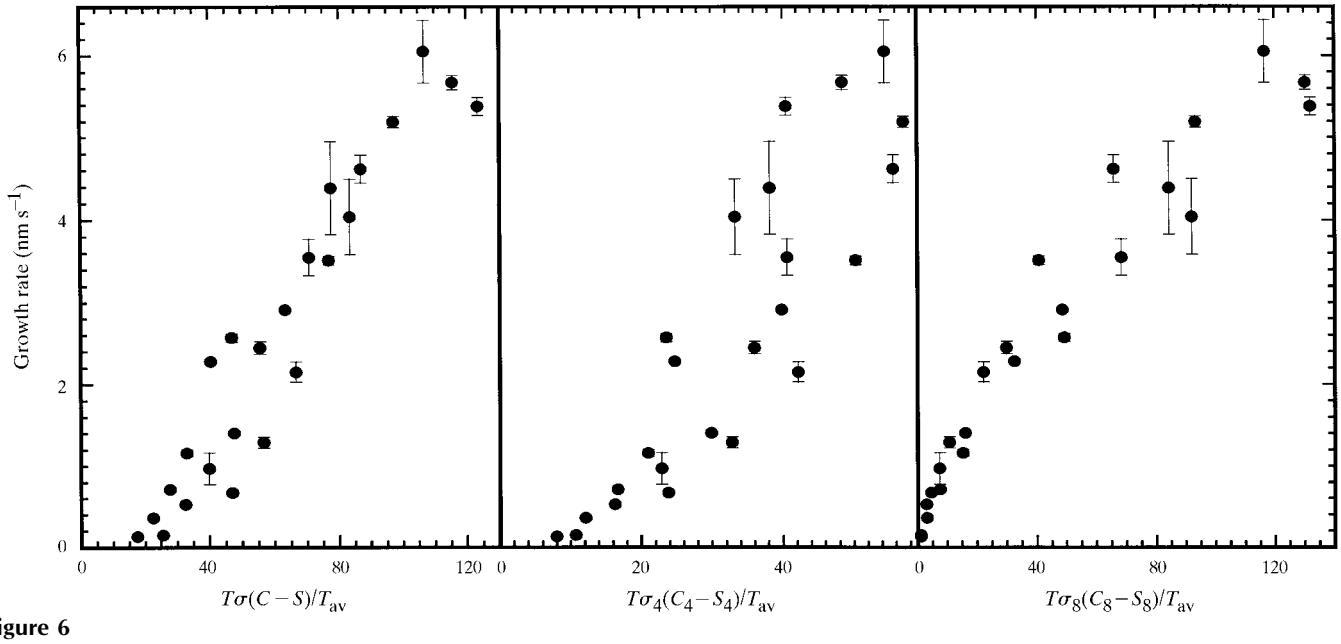

Figure 6
Plots of the measured macroscopic growth rates of the (101) face at pH 4.6, 3% NaCl. They are plotted for the functional relationships for dislocation growth by isolated hillocks given by (3)–(5): against $T\sigma(C-S)/T_{av}$ for monomer growth from monodisperse solutions and against $T\sigma_4(C_4-S_4)/T_{av}$ and $T\sigma_8(C_8-S_8)/T_{av}$ for tetramer and octamer growth from polydisperse solutions.

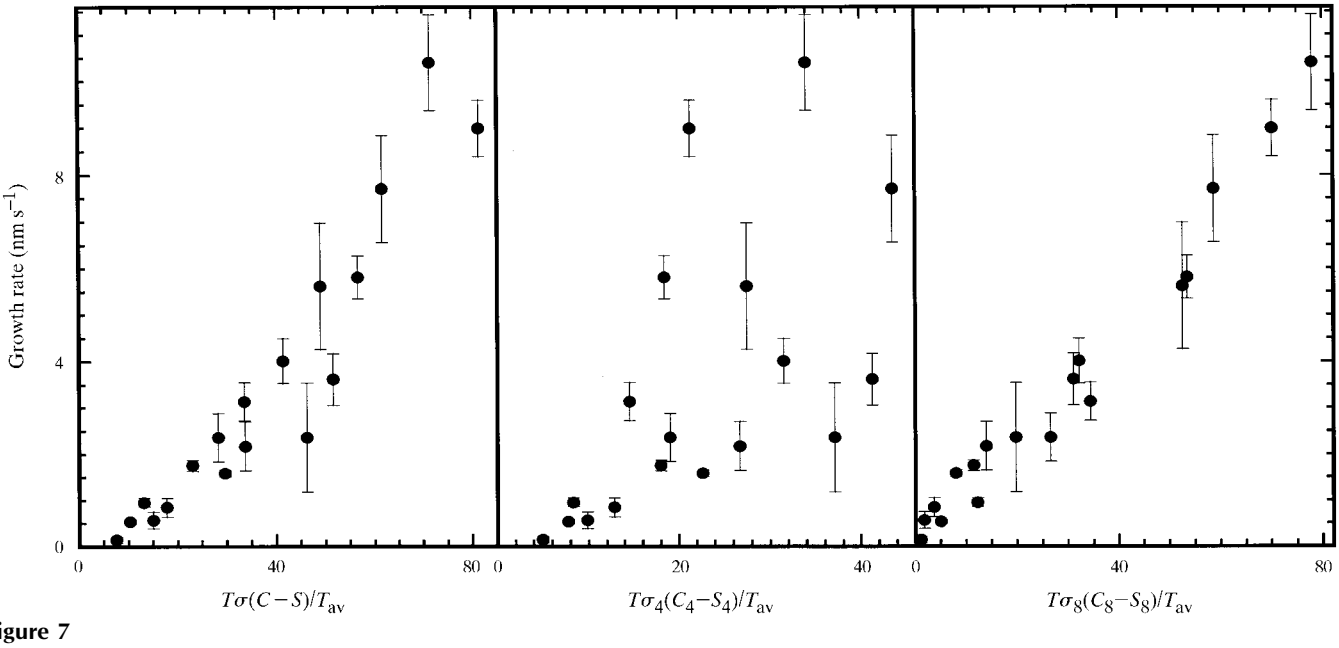

Figure 7
Plots of the measured macroscopic growth rates of the (101) face at pH 4.0, 5% NaCl. They are plotted for the functional relationships for dislocation growth by isolated hillocks given by (3)–(5): against $T\sigma(C-S)/T_{av}$ for monomer growth from monodisperse solutions and against $T\sigma_4(C_4-S_4)/T_{av}$ and $T\sigma_8(C_8-S_8)/T_{av}$ for tetramer and octamer growth from polydisperse solutions.

$\exp(-qT_{av}^2/T^2\sigma_4)$ for pH 4.0/5% NaCl and pH 5.0/5% NaCl, the data does not show discernible trends. Considering monomer growth for the case of pH 4.0/5% NaCl in Fig. 10, we can see that there is linear behavior at the lower σ. However, at supersaturations where two-dimensional nucleation is expected to prevail, the curve starts to deviate and even begins to decrease. When octamer growth is considered, we obtain the expected linear trend at high σ, suggesting that this is the averaged growth unit. Similar observations can be made for the case of pH 5.0/5% NaCl shown in Fig. 11. Assuming octamers to be the averaged growth units matches the expected trends the closest,

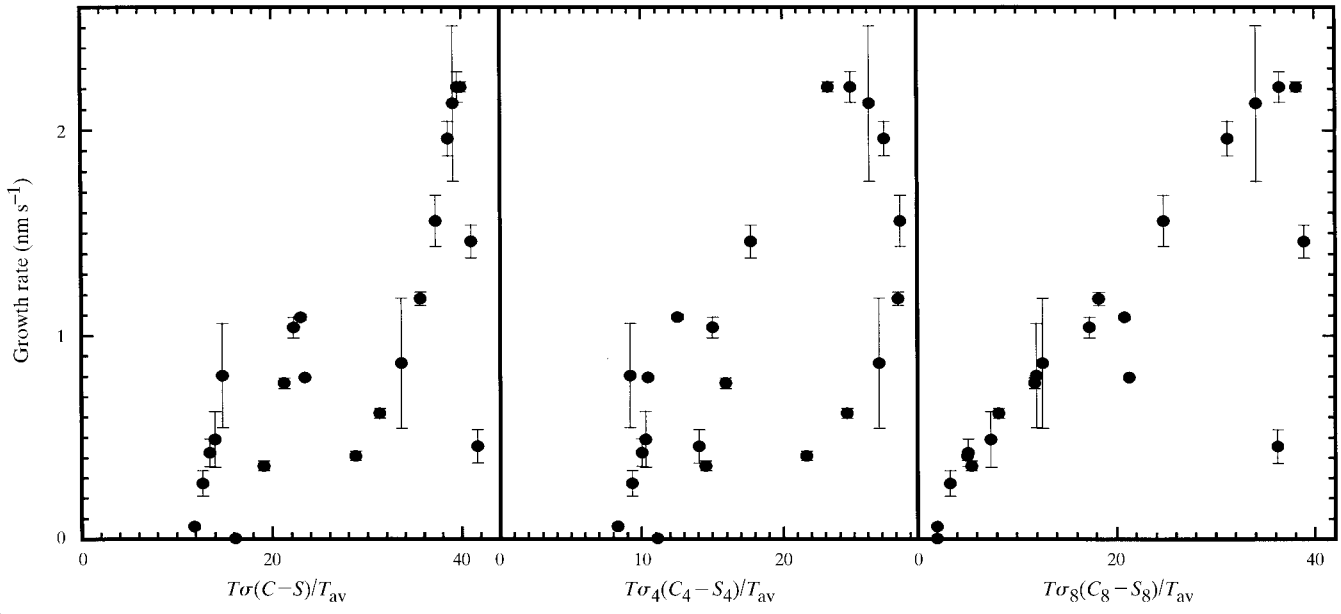

Figure 8
Plots of the measured macroscopic growth rates of the (101) face at pH 5.0, 5% NaCl. They are plotted for the functional relationships for dislocation growth by isolated hillocks given by (3)–(5): against $T\sigma(C-S)/T_{av}$ for monomer growth from monodisperse solutions and against $T\sigma_4(C_4-S_4)/T_{av}$ and $T\sigma_8(C_8-S_8)/T_{av}$ for tetramer and octamer growth from polydisperse solutions.

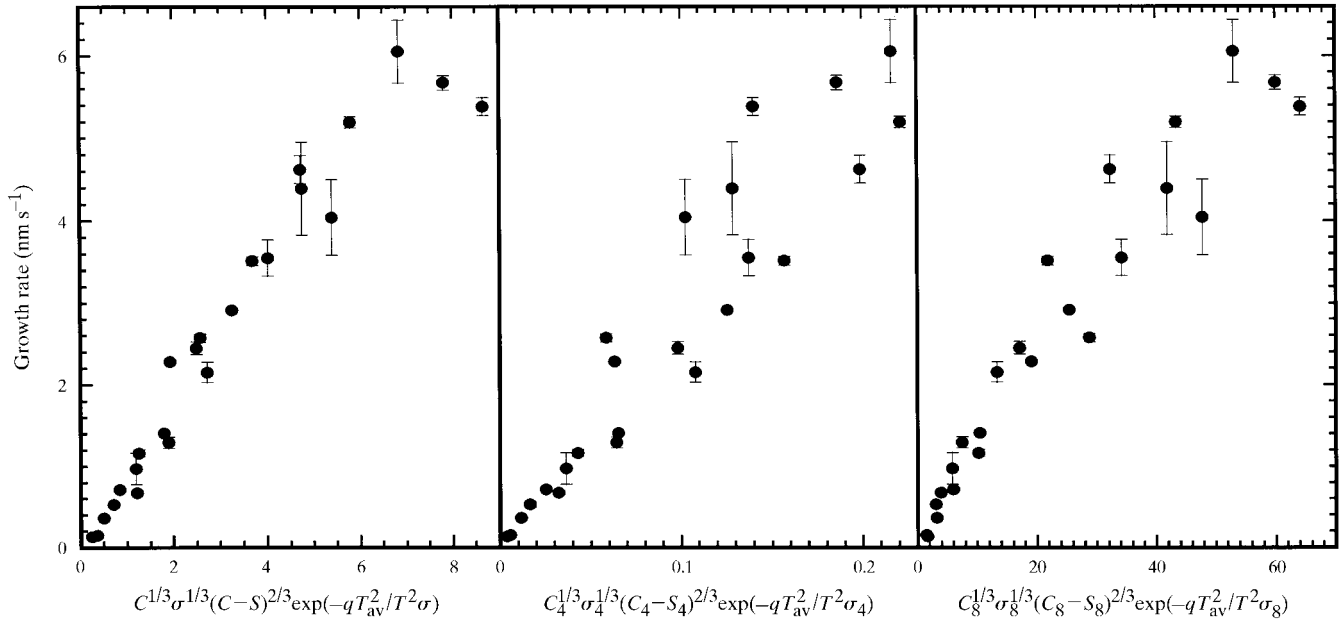

Figure 9
Plots of the measured macroscopic growth rates of the (101) face at pH 4.6, 3% NaCl. They are plotted for the functional relationships for two-dimensional nucleation growth given by (6): against $C^{1/3}\sigma^{1/6}(C-S)^{2/3}\exp(-qT_{av}^2/T^2\sigma)$ for monomer growth from monodisperse solutions and against $C_4^{1/3}\sigma_4^{1/6}(C_4-S_4)^{2/3}\exp(-qT_{av}^2/T^2\sigma_4)$ and $C_8^{1/3}\sigma_8^{1/6}(C_8-S_8)^{2/3}\exp(-qT_{av}^2/T^2\sigma_8)$ for tetramer and octamer growth, respectively, from polydisperse solutions. The values of q are obtained by first plotting $\ln[R/C_N^{1/3}\sigma_n^{1/6}(C_n-S_n)^{2/3}]$ against $T_{av}^2/T^2\sigma_n$ for each growth unit. They are 5.33, 21.59 and −12.18 for monomers, tetramers and octamers, respectively.

although there is somewhat greater scatter in the data compared with the other conditions.

The above results show that the growth of the (101) face proceeds by the addition of multimeric growth units through the dislocation and two-dimensional nucleation growth mechanisms. Monomer growth from monodisperse solutions does not adequately describe the growth process under any condition. This result is in agreement with

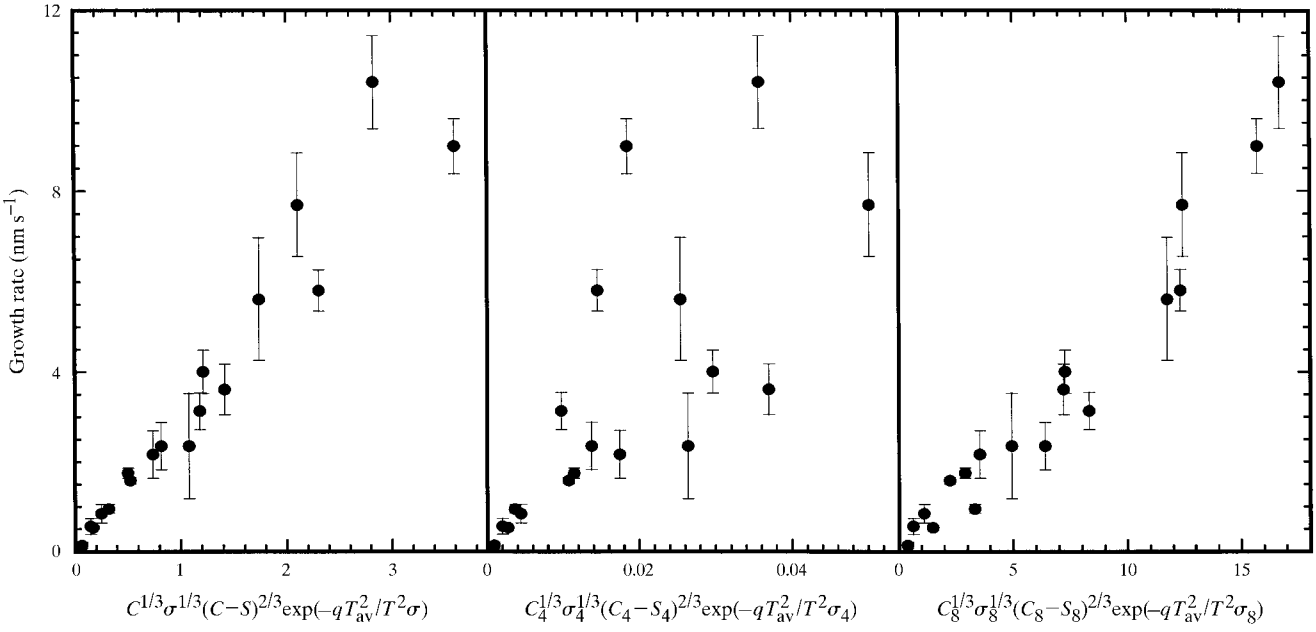

Figure 10
Plots of the measured macroscopic growth rates of the (101) face at pH 4.0, 5% NaCl. They are plotted for the functional relationships for two-dimensional nucleation growth given by (6): against $C^{1/3}\sigma^{1/6}(C-S)^{2/3}\exp(-qT_{av}^2/T^2\sigma)$ for monomer growth from monodisperse solutions and against $C_4^{1/3}\sigma_4^{1/6}(C_4-S_4)^{2/3}\exp(-qT_{av}^2/T^2\sigma_4)$ and $C_8^{1/3}\sigma_8^{1/6}(C_8-S_8)^{2/3}\exp(-qT_{av}^2/T^2\sigma_8)$ for tetramer and octamer growth, respectively, from polydisperse solutions. The values of q are obtained by first plotting $\ln[R/C_N^{1/3}\sigma_n^{1/6}(C_n-S_n)^{2/3}]$ against $T_{av}^2/T^2\sigma_n$ for each growth unit. They are 7.78, 33.32 and −7.21 for monomers, tetramers and octamers, respectively.

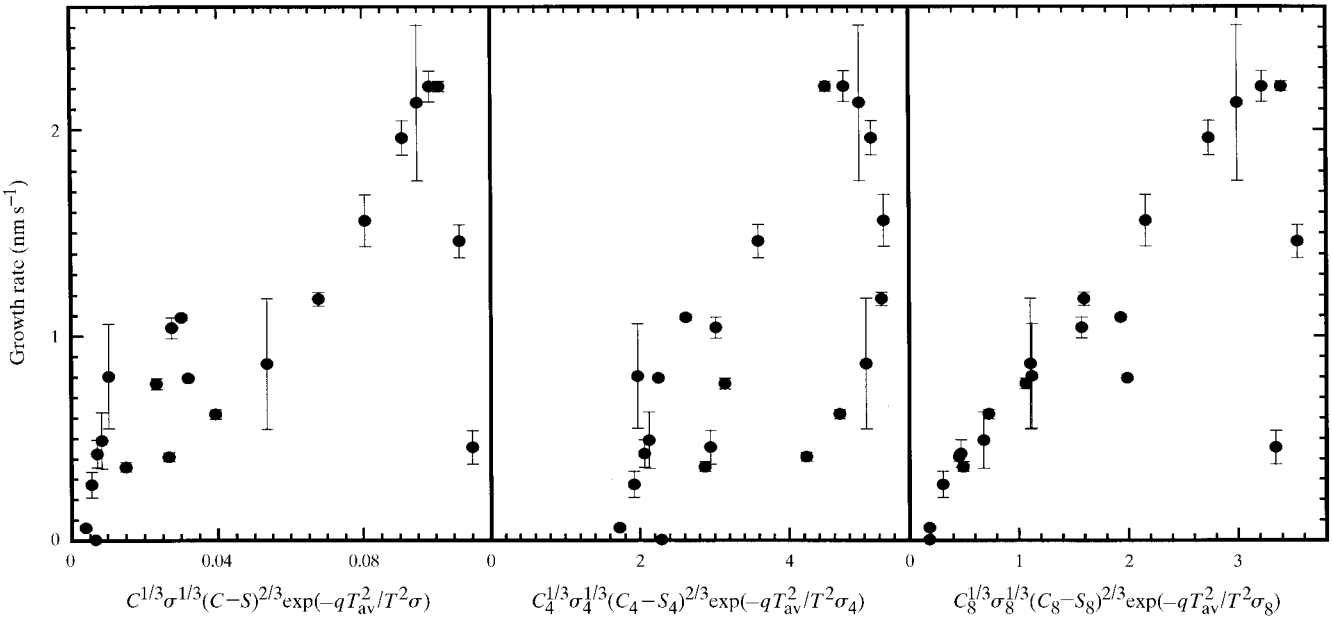

Figure 11
Plots of the measured macroscopic growth rates of the (101) face at pH 5.0, 5% NaCl. They are plotted for the functional relationships for two-dimensional nucleation growth given by (6): against $C^{1/3}\sigma^{1/6}(C-S)^{2/3}\exp(-qT_{av}^2/T^2\sigma)$ for monomer growth from monodisperse solutions and against $C_4^{1/3}\sigma_4^{1/6}(C_4-S_4)^{2/3}\exp(-qT_{av}^2/T^2\sigma_4)$ and $C_8^{1/3}\sigma_8^{1/6}(C_8-S_8)^{2/3}\exp(-qT_{av}^2/T^2\sigma_8)$ for tetramer and octamer growth, respectively, from polydisperse solutions. The values of q are obtained by first plotting $\ln[R/C_N^{1/3}\sigma_n^{1/6}(C_n-S_n)^{2/3}]$ against $T_{av}^2/T^2\sigma_n$ for each growth unit. They are 14.32, 1.54 and −26.19 for monomers, tetramers and octamers, respectively.

predictions made from molecular-packing arrangements. Unlike for the (110) face, a single averaged growth-unit size was not obtained for the (101) face under all conditions. Given the recent observation that growth occurs by multiple growth units on the (110) face, the good agreement obtained with octamer units for the growth of that face with the macroscopic model employing (1) can be regarded as a coincidence. Thus, it is not surprising that a similar agreement with a growth unit included in (1) was not obtained for the (101) face. Additionally, for almost all cases the agreement between the model and the data for the (101) face was much less than the excellent fits obtained for the (110) face. These observations suggest that the average growth-unit size which might produce the best agreement is one between a tetramer and an octamer, such as a hexamer or even a fractional unit. The formation of such units can no longer be conveniently represented by a series of reactions such as (1).

Such an intermediate unit would be in keeping with other observations and constraints on the (101) growth process. Firstly, the minimum growth-unit size for tetragonal lysozyme crystals is required to be a 4_3 helical tetramer. This means that for the average growth unit to be a tetramer, growth on the (101) face must proceed solely by tetramer addition. Instead, as discussed earlier, growth of this face is likely to proceed by a variety of units with tetramers as the minimum size. This will result in the averaged growth-unit size being larger than a tetramer. Secondly, as discussed previously, the surface structures of the two faces makes it more likely that the (101) face grows by smaller clusters. This suggests that the averaged growth-unit size for the (101) face is smaller than the octamer growth units of the (110) face.

These two constraints would cause the averaged growth unit to be an intermediate or fractional unit between tetramers and octamers and one not represented in (1). This is in keeping with the fits obtained with the data, as shown in Figs. 6–11. It is possible to modify (1) to include intermediate species, one of which may produce better agreement with the data. However, such a species would still only represent the average of all growth units participating in the (101) growth process and identifying it would not provide a significant improvement in our understanding of this process. Improved understanding can only be obtained from a time-resolved investigation of the molecular-growth process to individually identify the participating growth units, similar to that performed for the (110) face (Li, Nadarajah *et al.*, 1999).

Despite its limitations, the macroscopic model employed here serves the useful purpose of suggesting that the average size of the growth unit for the (101) face is between a tetramer and an octamer. This explains the observations that the (101) face grows faster than the (110) face at lower supersaturations and grows slower than the (110) face at higher supersaturations. The equilibrium in (1) ensures that smaller lysozyme clusters will predominate at the lower supersaturations and the larger ones at the higher supersaturations. Thus, it is obvious that the growth of different faces will be favored depending on the supersaturation employed.

5. Conclusions

The (101) face of tetragonal lysozyme crystals is quite irregular, making it more difficult to construct the molecular-packing arrangement and the molecular-growth mechanism. Fortunately, AFM and electron-microscopy scans have allowed us to verify the constructed arrangements ensuring their validity. The correct packing arrangement contains only complete 4_3 helices, resulting in a molecularly rough face with edge-to-edge dimensions corresponding to unit-cell dimensions. The predicted molecular-growth mechanism for this face involves the formation of single unimolecular growth layers by the addition of 4_3 tetramer growth units. However, the molecular roughness of the (101) face shown by these analyses also implies that it facilitates growth not just by tetramer addition, but by the addition of other aggregate species and impurities as well. These result in the formation of multi-layered growth steps, allowing growth to proceed by units larger than the basic tetramer unit. Thus, growth is likely to involve several growth units similar to that observed for the (110) face, resulting in an averaged growth unit which is larger than a tetramer.

However, unlike the (110) face, the surface structure of the (101) face will restrict the variety of growth units to the smaller ones. This means that the averaged growth unit for the (101) is smaller than an octamer and explains the relative growth rates of the (101) and (110) faces at higher and lower supersaturations. The macroscopic model which was employed in this study, involving the addition of different growth units to the (101) face by dislocation and two-dimensional nucleation growth, indicates that the average size of the growth unit is indeed between a tetramer and an octamer.

This work was supported by grants NAG8-984 and NCC8-134 from the NASA/Marshall Space Flight Center. Partial support for Ms Meirong Li from the College of Engineering of the University of Toledo during the course of this study is also acknowledged.

References

Behlke, J. & Knespel, A. (1996). *J. Cryst. Growth*, **158**, 388–391.
Cacioppo, E. & Pusey, M. L. (1991). *J. Cryst. Growth*, **114**, 286–292.
Chernov, A. A. (1984). *Crystal Growth.* Berlin: Springer.
Chernov, A. A. (1988). *Contemp. Phys.* **30**, 251–276.
Durbin, S. D. & Carlson, W. E. (1992). *J. Cryst. Growth*, **122**, 71–79.
Durbin, S. D. & Feher, G. (1986). *J. Cryst. Growth*, **76**, 583–592.
Durbin, S. D. & Feher, G. (1990). *J. Mol. Biol.* **212**, 763–774.
Forsythe, E. L., Nadarajah, A. & Pusey, M. L. (1999). *Acta Cryst.* D**55**, 1005–1011.
Konnert, J. H., D'Antonio, P. & Ward, K. B. (1994). *Acta Cryst.* D**50**, 603–613.
Li, M., Nadarajah, A. & Pusey, M. L. (1995). *J. Cryst. Growth*, **156**, 121–132.
Li, H., Nadarajah, A. & Pusey, M. L. (1999). *Acta Cryst.* D**55**, 1036–1045.
Li, H., Perozzo, M. A., Konnert, J. H., Nadarajah, A. & Pusey, M. L. (1999). *Acta Cryst.* D**55**, 1023–1035.
Minezaki, Y., Nimura, N., Ataka, M. & Katsura, T. (1996). *Biophys. Chem.* **58**, 355–363.

Nadarajah, A., Forsythe, E. L. & Pusey, M. L. (1995). *J. Cryst. Growth*, **151**, 163–172.
Nadarajah, A., Li, M. & Pusey, M. L. (1997). *Acta Cryst.* D**53**, 524–534.
Nadarajah, A. & Pusey, M. L. (1996). *Acta Cryst.* D**52**, 983–996.
Pusey, M. L. (1991). *J. Cryst. Growth*, **110**, 60–65.
Steinrauf, L. K. (1959). *Acta Cryst.* **12**, 77–79.
Strom, C. S. & Bennema, P. (1997*a*). *J. Cryst. Growth*, **173**, 150–158.
Strom, C. S. & Bennema, P. (1997*b*). *J. Cryst. Growth*, **173**, 159–166.
Wilson, L. J., Adcock-Downey, L. & Pusey, M. L. (1996). *Biophys. J.* **71**, 2123–2129.
Young, A. C., Tilton, R. F. & Dewan, J. C. (1994). *J. Mol. Biol.* **235**, 302–317.